Scintigraphic Detection of Congenital Intracranial Vascular Malformations

Gary F. Gates, Lawrence S. Fishman, and Hervey D. Segall

Childrens Hospital of Los Angeles, Los Angeles, California

Nine children with arteriovenous malformations (AVMs), and a tenth with a cerebral aneurysm, had computer-processed dynamic scintigraphy with static scintigrams, transmission computed tomography (CT) both with and without contrast injection, and radiopaque cerebral angiography. All ten lesions were detected by dynamic scintigraphy and angiography, whereas two AVMs were missed on CT scans and the aneurysm and two AVMs (one missed by CT) were not identified on static scintigrams. Time-activity curves generated from regions of interest placed over the cerebral hemispheres, AVMs and/or various venous structures permitted, respectively, estimation of interhemispheric partition of perfusion, estimation of the fraction of total cerebral hemispheric perfusion preferentially directed into a malformation, and indication of the route of venous drainage from the lesions. While dynamic scintigraphy and CT scanning both identified the aneurysm, scintigraphy was the most effective screening test for detecting AVMs owing to its accuracy, lower cost, and lack of required anesthesia, heavy sedation or iodinated contrast agents.

J Nucl Med 19: 235–244, 1978

Reliable detection of congenital intracranial arteriovenous malformations (AVMs) and aneurysms is important because the prognosis for these conditions has improved with advances in neurosurgery. Cerebral angiography is necessary before intracranial surgery for such lesions but is not suitable as a widespread screening test because it is an expensive, time-consuming procedure with some associated risk. Radionuclide cerebral studies have been used in the past to detect these vascular, non-neoplastic abnormalities. In addition, another relatively "noninvasive" screening test, transmission computed tomography (CT), is now available. Consequently nine children with AVMs, and a tenth with a cerebral aneurysm, were evaluated with radionuclide scintigraphy and CT scanning to determine which was the more effective screening test.

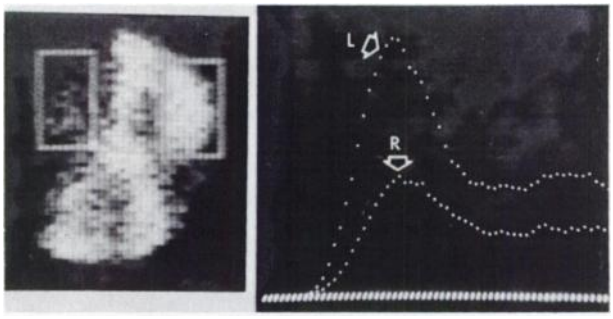

FIG. 1. Fifteen-year-old girl (Patient 5) with left frontal AVM. Anterior dynamic study shows equal rectangular ROIs placed over cerebral hemispheres, avoiding midline vessels and superior sagittal sinus and its afferent veins. Time-activity curves (each point 0.5 sec) plot hemispheric tracer passage; left side received 72% of initial first-pass nuclide flow; right, 28%.

Received July 21, 1977; revision accepted Sept. 20, 1977.

For reprints contact: Gary F. Gates, Div. of Nuclear Medicine, Childrens Hospital of Los Angeles, P.O. Box 54700, Los Angeles, CA 90054.

MATERIALS AND METHODS

Seven girls and two boys with AVMs, ranging in age from 3 to 19 yr (average, 12.8), and a 2½-year-old boy with a cerebral aneurysm, were studied by radionuclide scintigraphy, CT scanning, and cerebral angiography (Table 1). Following a rapid i.v. administration of Tc-99m, diethylenetriamine-pentaacetic acid (DTPA, 0.28 mCi/kg, minimum 2 mCi), cerebral scintiangiography was performed using a scintillation camera interfaced to a digital computer. Seven studies were performed in the anterior projection; three used the posterior because a posterior abnormality was suspected clinically. The child with the cerebral aneurysm had both anterior and posterior dynamic studies on successive days.

Cerebral perfusion was also evaluated by cerebral hemispheric time-activity curves that depicted the tracer's passage through the brain. Equal rectangular regions of interest (ROIs) were manually assigned over each hemisphere. The superior sagittal sinus and its associated large afferent veins near the superior cortical borders were avoided, as were the midline vascular structures including anterior cerebral arteries, deep venous sinuses, and circle of Willis (Fig. 1). Initial interhemispheric nuclide distribution was estimated by integrating each curve from the upswing (at twice background count) to the time at which the first of the pair reached its peak; each integral was then expressed as a percentage of the sum of both. Supratentorial AVMs could also be identified separately by a cursor; and their curves could be compared with the total cerebral hemispheric curves, in the same manner as indicated above, to estimate the percentage of initial total hemispheric tracer located within a malformation. The formula below summarizes this step.

TABLE 1. SCINTIGRAPHIC AND RADIOLOGIC ASSESSMENT OF CONGENITAL VASCULAR LESIONS IN CHILDREN

	Scintigraphic image		Distribution of initial 1st-pass perfusion		CT scan	
Angiographic abnormality	Dynamic	Static	% L-R cerebral hemispheres	% AVM*-% cerebral hemispheres	Precontrast	Postcontrast
(1) AVM, RMCA (19 y/o, F)	AVM, RMCA	Pos	48–52†	34–66	R porencephaly	n/c
(2) AVM, LSCA (15 y/o, F)	AVM, L posterior fossa	Neg	42–58‡	——	Ventricular hemorrhage	n/c
(3) AVM's mult. (Wyburn-Mason syndrome, 12 y/o, F)	AVM, midline, post. fossa	Pos (multiple foci)	59–41‡	——	Cerebral calcifications	Vascular enhancement of multiple foci
(4) AVM, great cerebral vein of Galen malformation (3 y/o, F)	AVM, midline with bilateral ↓ cerebral perfusion	Pos	54–46† (May, 1976) 51–49† (June, 1977)	65–35 69–31	Cerebral calcifications; mass distorting 4th ventricle	Vascular enhancement of periventricular mass
(5) AVM, left frontal-parietal (Rendu-Osler-Weber syndrome) (15 y/o, F)	AVM, left frontal	Pos	72–28†	41–59	↑ and ↓ densities	Vascular enhancement
(6) AVM, LACA (5 y/o, M)	AVM, L frontal	Pos	87–13†	43–57	Neg	Vascular enhancement
(7) AVM, RPICA (15 y/o, F)	AVM, R posterior fossa	Pos	50–50‡	——	Cerebral calcifications	Vascular enhancement
(8) AVM, deep branches LMCA (17 y/o, M)	AVM, deep L frontal	Pos	71–29†	42–58	Neg¶	Vascular enhancement
(9) AVM, deep branches RMCA (14 y/o, F)	AVM, deep R frontal	Neg	38–62†	32–68	R ventricular hemorrhage	Vascular enhancement
(10) Aneurysm RPCA (2½ y/o, M)	Vascular mass, R cerebral	Neg	49–51† 47–53‡	——	Mass with ↑ density	Vascular enhancement

* = only supratentorial AVMs; † = anterior dynamic study; ‡ = posterior dynamic study; ¶ = incidental effects of previous posterior-fossa surgery for brain tumor seen; n/c = no change; RMCA = Right middle cerebral artery; LSCA = Left superior cerebellar artery; LACA = Left anterior cerebral artery; RPICA = Right posterior inferior cerebellar artery; LMCA = Left middle cerebral artery; RPCA = Right posterior cerebral artery.

$$\%\ \text{initial tracer located in AVM} = \frac{\text{integral* AVM counts}}{\text{integral* total cerebral hemispheric counts}} \times 100.$$

Additional ROIs could be placed over an AVM as well as contiguous venous structures in order to determine the time sequence of the tracer's appearance in these selected areas, thereby indicating the route of probable venous drainage from the malformation.

At least one static analog scintigram was obtained 1 min after nuclide administration, at which time multiple views could be obtained rapidly if desired. Following a 20- to 30-min delay, a full static scintigraphic sequence was performed in as many projections as the patient's condition would allow—preferably anterior, posterior, both laterals, vertex, and occasionally oblique views. Static scintigraphy was performed using a parallel-hole collimator and accumulating 300,000 counts per image.

CT brain scanning was performed using a scanner with a 160 × 160 matrix. The 1.3-cm tomographic sections were performed parallel to a plane 15° from Reid's base line. Scans were obtained both before and after the iodinated contrast administration, the latter using a bolus injection of iothalamate (60%, 2 ml/kg). The first tomographic section was quickly started at the level of a suspected lesion.

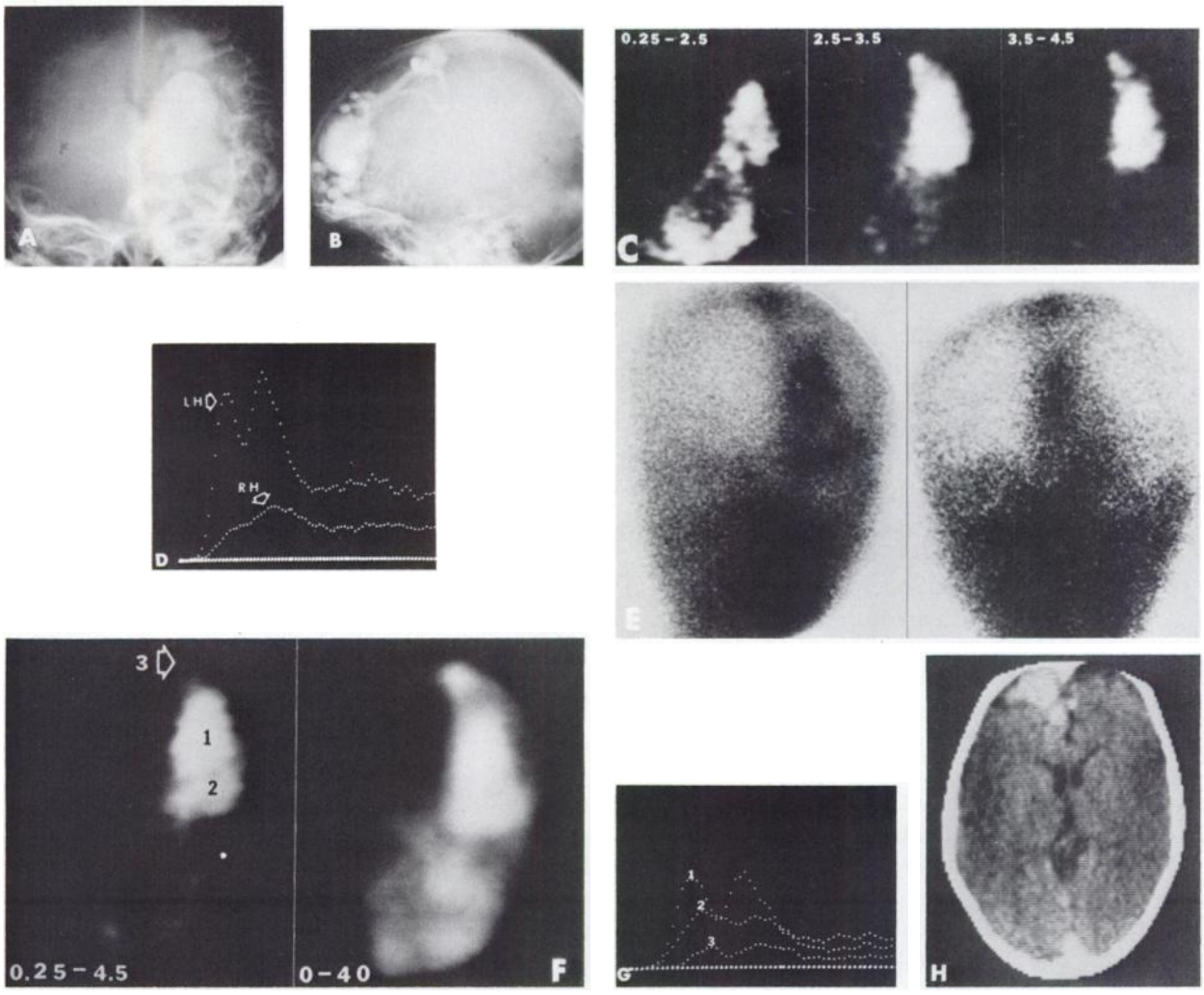

FIG. 2. Five-year-old boy (Patient 6) with AVM arising from left anterior cerebral artery (LACA). A-P cerebral angiogram (A) shows AVM fed from LACA. Route of venous drainage was lateral and inferior, with a vein eventually ascending medially to join superior sagittal sinus (lateral radiogram, B). Anterior dynamic scintigraphy (C) with time intervals (sec) indicated, shows left frontal AVM. Curves (D, 0.25 sec/point) show 87% of initial tracer in left hemisphere (LH). LH curve has earlier peak and more rapid recirculation than RH, with curve separation persisting through entire study. (E) Anterior views: sixty-second postinjection (left) and 30-min delayed (right) also show AVM. Route of venous drainage evaluated by placing ROIs (F) over its components (Areas 1, 2) and superior sagittal sinus (#3). Peaks of corresponding curves (G) show sequence of tracer appearance in these regions, confirming that AVM initially drains inferiorly before its content reaches superior sagittal sinus. (H) CT scan after contrast injection shows left frontal AVM, which was not identified on precontrast scans.

RESULTS

All ten congenital vascular malformations were detected by dynamic scintigraphy, but only eight were identified by CT scanning. The specific results of these two tests are summarized in Table 1 and presented below.

Radionuclide cerebral scintigraphy. Dynamic scintigraphy was the most valuable portion of the radionuclide examination, since all vascular malformations were best seen in this phase of the study. All but one of the AVMs (Case 9) were still identifiable on the 1-min postinjection static image, but the aneurysm was barely seen, if at all. Static scintigraphy delayed 20–30 min detected seven of the abnormalities but was normal in three patients: a 15-year-old girl (Case 2) with an AVM originating from the left superior cerebellar artery; a 14-year-old girl (Case 9) with an AVM originating from the right middle cerebral artery; and a 2½-year-old boy (Case 10) with an aneurysm arising from the right posterior cerebral artery.

Four AVMs were clearly located within one cerebral hemisphere (Cases 5, 6, 8, 9), producing an enormous maldistribution of radionuclide, with scintigraphic images showing much of the perfusion diverted into the affected side. In such circumstances analysis of the cerebral hemispheric curves showed the involved side receiving from 62 to 87% of initial first-pass tracer distribution (Fig. 2). In these circumstances the AVM alone accounted for up to 43% of the initial radionuclide within both cerebral hemispheres (Table 1). A fifth patient (Case 1, Fig. 3), in whom scintigraphy showed an enormous AVM within one cerebral hemisphere, had nearly symmetrical initial hemispheric tracer distribution by curve analysis. This paradox resulted from porencephaly (evident by CT scanning) coexisting in the same hemisphere as the AVM (not seen by CT scanning). The loss of normally perfused brain tissue was offset by the AVM's increased perfusion. Following surgical removal of this AVM, repeat scintigraphy and curve analysis showed the hypoperfusion of the porencephalic hemisphere. A sixth child (Case 2), with a posterior-fossa AVM, had diminished initial radionuclide distribution (evident by scintigraphy and curve analysis) in the left cerebral hemisphere due to cerebral infarction that followed a ventricular hemorrhage.

Bilaterally diminished cerebral hemispheric perfusion, involving the right side more than the left, occurred in a 7th child, who had multiple intracranial AVMs in association with the Wyburn-Mason syndrome (Case 3). Dynamic scintigraphy showed the most hemodynamically significant lesion to be a large mesencephalic AVM. The eighth child had a malformation of the great cerebral vein of Galen (Case 4, Fig. 4), with massive shunting of radionuclide directly through the anomalous arterial connections into the aneurysmally enlarged vein. Severe hypoperfusion of both hemispheres was seen by scintigraphy, with curve analysis showing both sides nearly equally affected. When a cursor was placed over the venous malformation, the resulting curve showed the rapid perfusion of the vascular lesion and analysis indicated that some 69% of the initial intracranial radionuclide seen on the anterior dynamic study was being diverted into the malformation. The hemispheric hypoperfusion delayed imaging of the superior sagittal sinus until the 7- to 9-sec scintiphoto; this represents a 3-sec delay in the normal imaging sequence.

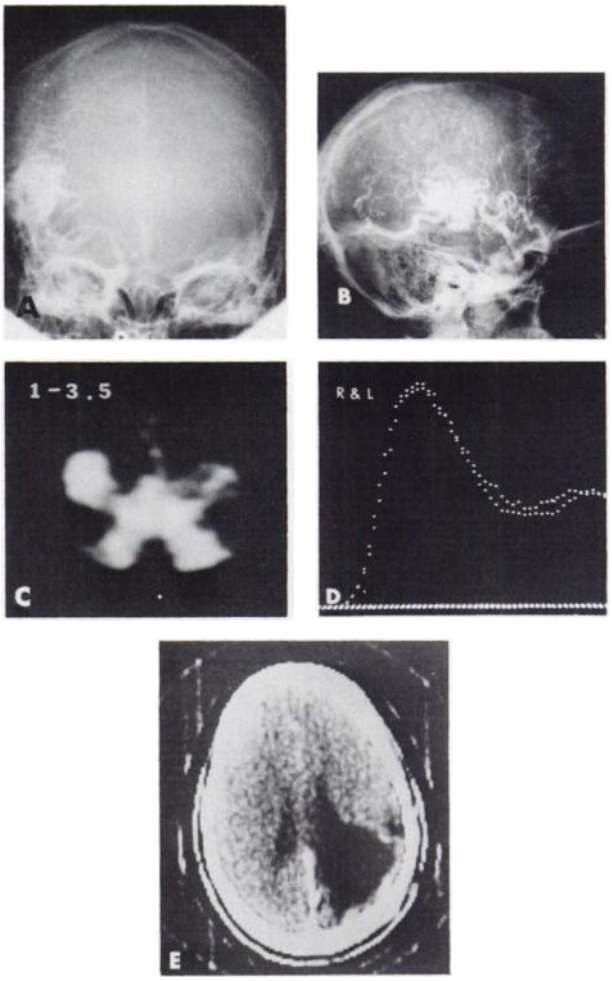

FIG. 3. Nineteen-year-old girl (Patient 1) with AVM arising from right middle cerebral artery (RMCA). A-P cerebral angiogram (A) shows AVM fed by RMCA. Lateral angiograms (B) show AVM draining anteriorly and posteriorly but not into superior sagittal sinus. Anterior dynamic study (C) shows AVM associated with RMCA while cerebral hemispheric curves (D), show tracer distribution surprisingly similar. CT scan (E) after contrast injection disclosed porencephaly (explaining the curves) but failed to show the AVM.

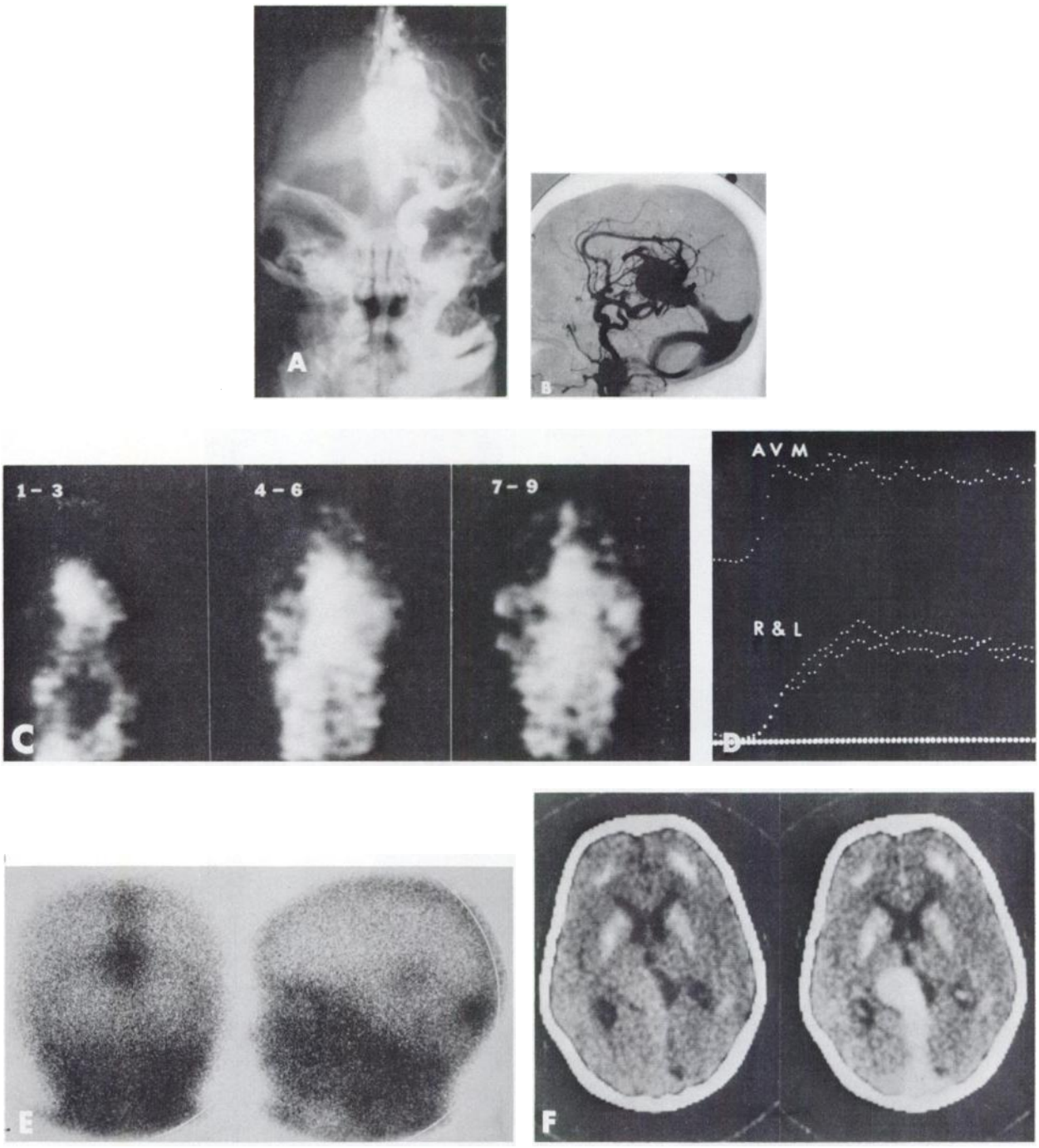

FIG. 4. Three-year-old girl (Patient 4) with great cerebral vein of Galen malformation. AP cerebral angiogram (A) with subtraction lateral (B) show prompt flow into great cerebral vein of Galen from carotid system (including a persisting trigeminal artery). Venous drainage was into straight sinus and torcular Herophili; superior sagittal sinus was not in main drainage route. Anterior dynamic study (C) shows vascular midline malformation, diminished appearance of tracer in cerebral hemispheres, and delayed imaging of superior sagittal sinus until the 7- to 9-sec interval. Curves (D) show nearly equal hemispheric perfusion (R & L) while the AVM is more promptly perfused (base line shifted upward for display purposes). Delayed static scintigrams (E, posterior and left lateral) show the malformation. CT scans before and after contrast injection (F) show cerebral calcifications and distortion of left side of quadrageminal cistern by a mass whose vascular nature was demonstrated by iothalamate.

The ninth AVM (Case 7) was located in the posterior fossa and did not produce abnormalities of cerebral hemispheric perfusion that could be detected by either scintigraphic imaging or curve analysis.

The tenth child (Case 10, Fig. 5) had an aneu-

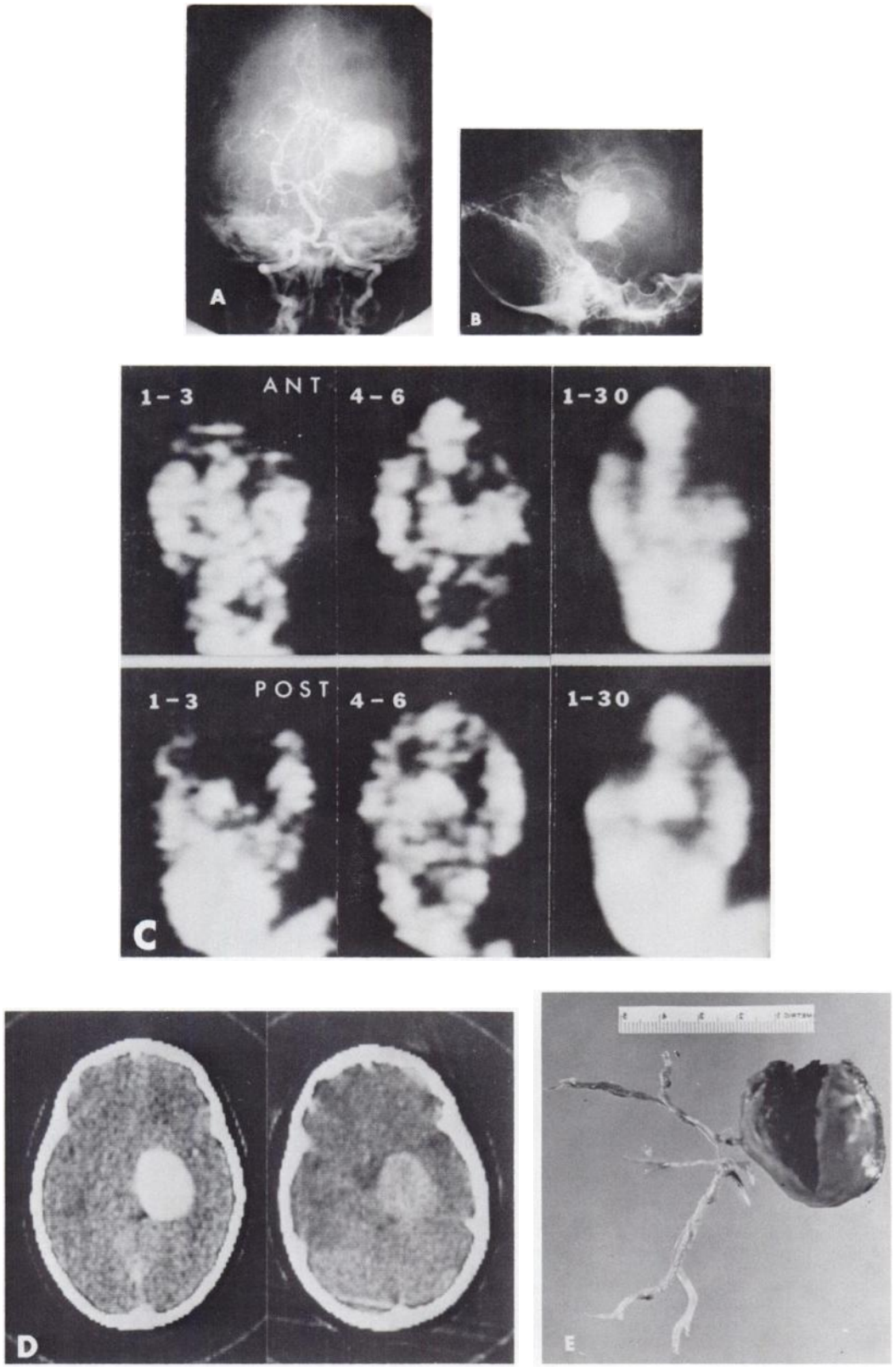

FIG. 5. Boy, aged 2½ yr, (Patient 9) with aneurysm arising from right posterior cerebral artery (RPCA). AP vertebral angiogram (A), reversed to be similarly oriented to posterior scintigram and CT scan, shows jetting of contrast into aneurysm from RPCA. A late lateral view (B) shows retention of contrast in aneurysm long after surrounding veins had emptied. (C) Anterior and posterior dynamic scintigrams show vascular lesion on right (not to be mistaken for torcular Herophili on posterior study). (D) CT scan immediately following contrast injection, and another 4½ hr later, show aneurysm. (E) Aneurysm ruptured the night before surgery. Its size and location were dramatically demonstrated at autopsy, when the circle of Willis was dissected and removed.

rysm arising from the right posterior cerebral artery. A hypervascular region was seen on both anterior and posterior dynamic studies, but both curve analyses from the examinations showed that the two hemispheres had almost equal radiotracer distributions.

The route of venous drainage from an AVM could also be assessed by dynamic scintigraphy (Fig. 2). ROIs could be placed over selected components of an AVM and the great veins in order to determine the time sequence of radionuclide passage through these structures. Of course, if venous drainage occurred directly posterior to the plane in which an AVM was being imaged, such curve analysis could not be done (Fig. 3). The condition could be suspected, however, from the appearance of the scintigraphic images as in the case with malformation of the great cerebral vein of Galen (Fig. 4).

CT scanning. Overall, eight of ten vascular lesions were detected by CT scanning, whereas two AVMs (Cases 1, 2) were missed. Scans obtained before contrast administration were normal in two patients (Cases 6, 8); showed intracerebral calcifications in three (Cases 3, 4, 7); identified displacement of normal structures by a mass in two (Cases 4, 9); showed porencephaly in one (Case 1); and displayed ventricular hemorrhage in two cases (Cases 2, 9). In only two patients, however, was a vascular mass directly suspected (Cases 5, 10).

Following contrast administration, enhancement of vascular lesions occurred in eight patients (Cases 3–10) but not in two (Cases 1, 2). These last two children had prominent AVMs, demonstrated by dynamic radionuclide scintigraphy and cerebral angiography. One patient (Case 1) had porencephaly in the same hemisphere as the AVM; this was probably secondary to either intracerebral hemorrhage in the past and/or a previous neurosurgical attempt to remove her lesion. A second patient (Case 2) had an associated ventricular hemorrhage and cerebral infarction.

DISCUSSION

Intracranial perfusion can be assessed by dynamic scintigraphy using Tc-99m DTPA, since this nondiffusible tracer remains within the vascular space. The amount of radionuclide present in a region at any specific time is a complex function of the regional blood flow, local blood volume, and concentration of radionuclide in the portion of the bolus injection that arrived at that moment (*1*). Strictly speaking, cerebral scintiangiography using a nondiffusible tracer is not a quantitative "flow study," although regions of the brain with either high or low flow rates can be detected. Computer processing of images further improves the diagnostic quality of the examination. The method of scintigraphic image processing used in this series has been presented elsewhere (*2*).

There cerebral hemispheres or their subdivisions can be identified as areas of interest for the purpose of creating time-activity curves, which are analyzed in order to obtain more information regarding regional brain perfusion. These curves are composed of an initial rapid upstroke portion reflecting early tracer appearance ("wash-in") during the arterial phase, followed by a down slope of the curve from its peak value ("wash-out") as the tracer drains out during the venous phase. This "first-pass" curve is then followed by a "recirculation curve" which appears before tracer washout is complete. Normally curves from the two hemispheres are alike, whereas an ischemic hemisphere will have a curve with a slower upstroke and lower peak than the contralateral normal side, whereas the opposite will occur (i.e., rapid upstroke and higher peak) if the hemisphere contains an AVM (*3*).

A digital computer can further analyze the hemispheric curves resulting in circulation patterns related to various disease states (*4*). The technique used in this series was based on Sapirstein's principle (*5*) that the initial distribution (i.e., just after arterial delivery and before venous drainage) of a tracer that is ejected by the left ventricle reflects the fraction of cardiac output delivered to that organ. Moses et al. (*6*) applied this principle in analyzing cerebral curves during the early arterial phase by integrating the portion of both curves extending from twice background to the time at which the first of the pair reaches its peak value, and expressing the results as a ratio of left/right integral counts. Normals had left/right ratios of 1.00 ± 0.100 (1 s.d.), whereas 74% of abnormals had ratios beyond 2 standard deviations from the normal mean. Moses' technique is related to the microsphere distribution method of measuring relative regional perfusion; the early parts (i.e., first 12 sec) of cerebral histograms are identical for Xe-133, pertechnetate, and microspheres (*7*).

AVMs comprise less than 4% of all intracranial mass lesions and usually present in the second decade, with males being more often affected than females (*8*). Nearly 50% of all the patients are symptomatic before age 30 (*9*). Recurrent focal seizures of increasing frequency are the commonest presenting symptoms and occur in nearly 50% of the patients, with the rest presenting intraparenchymal and/or subarachnoid hemorrhages (25–50% incidence), cranial bruits (10–25% incidence), migrainous headaches, aphasia, hemianopsia, or hemi-

plegia resulting from cerebral ischemia (*8–10*). AVMs with large arteriovenous shunting may be associated with tachycardia, cardiomegaly, and cardiac failure. Craniomegaly may occur in children (*11*).

AVMs are predominantly located within the distribution of the middle cerebral artery, although they can occur in other locations. They can be fed from several arterial systems including the contralateral vasculature (*8,10*). These lesions are composed of irregular vascular channels formed by closely clustered arteries and tortuous draining veins. The main arteries supplying the malformations—and especially the veins draining them—are greatly dilated. Malformation of the great cerebral vein is an extreme example of the venous dilatation that occurs if one or more of the carotid or vertebral branches should communicate directly with this major, deep draining vessel. (It originates from the union of the basal vein of Rosenthal and the internal cerebral veins, and empties into the straight sinus.) When involved in a malformation the great cerebral vein of Galen enlarges to the point of resembling a saccular aneurysm; the straight sinus and torcular Herophili are also enlarged (*11,12*). AVMs situated over the cortical surface are triangular or conical in shape with the apex directed inward toward deeper portions of the brain.

Usually the circulation time through an AVM is abnormally short. It may approach normal values, however, in very large lesions presumably due to the increased length of the abnormal vessels and turbulent blood flow within their cavernous interior (*8,13,14*). Blood flow within AVMs may amount to four times the normal minute volume with the increase proportional to the size of the lesion; in these circumstances cardiac symptoms are more like to occur (*8,15–17*).

Dynamic cerebral scintigraphy has commonly been recognized as an effective means of detecting AVMs, with up to a 100% accuracy in some series (*18*). The malformations are identified as highly vascular lesions that promptly diminish in intensity due to venous drainage. Static scintigraphy can also detect 76–92% (*18,19*) of AVMs, although this detection rate drops to 60% for lesions less than 7 ml in volume (*19*). The detection rate of static examinations decreases as the interval between injection and onset of scintigraphy increases (*8*), a situation contrary to that occurring with successful imaging of brain tumors (*20*), except possibly the meningiomas. The venous (and possibly arterial) vessels can produce streaks on static images, and this is considered a useful diagnostic sign (*18,19*).

Of the intracranial aneurysms, 70–80% are congenital, with 83% located on the carotid portion of the circle of Willis and 17% on the vertebral portion (*10,21*). Few aneurysms are detected before age 20. Congenital aneurysms have a slightly higher frequency in females. They are multiple 20% of the time. They present either as a subarachnoid hemorrhage and/or possible intraparenchymal hematoma, or with clinical symptoms related to ischemia or to the direct pressure of the aneurysmal mass upon surrounding structures. Dynamic scintigraphy may show an early, transient, vascular lesion persisting for only a few seconds and suggestive of an arteriovenous malformation. On occasion it may be seen on static images (*10*).

All children in this series had vascular abnormalities detected by dynamic scintigraphy. All but one of the AVMs were still identifiable on the 1-min postinjection static scintigrams but the relative intensity of the abnormality diminished from the immediately preceding dynamic study. The aneurysm was barely if at all identifiable on the 1-min study. Seven of nine AVMs were still evident on the 20- to 30-min delayed views, but the abnormal areas were less obvious than on images obtained earlier. Two AVMs and the aneurysm could not be seen on delayed views.

Curve analysis helped to document the magnitude of the maldistribution of intracranial flow. Hyperperfusion of a cerebral hemisphere could occur when it contained an AVM, whereas bilateral hemispheric hypoperfusion occurred with deep, midline AVMs. The distribution of hemispheric perfusion appeared to be less affected by the cerebral aneurysm than by AVMs. In the presence of multiple AVMs, the one of greatest hemodynamic consequence was preferentially imaged (Case 3). The estimation of initial first-pass interhemispheric tracer distribution showed the largest flow imbalance occurring in a child (Patient 6) who presented with tachycardia and a left-ventricular strain pattern on electrocardiogram. In this and similar patients the percentage of radionuclide within an AVM accounted for much of the initial tracer within the cerebral hemispheres (Table 1). In such circumstances, maintenance of normal blood flow to the remaining cerebral areas could be achieved only by increasing total brain blood flow and cardiac output. Although all AVMs were visually identifiable on the dynamic scintigrams, curve analysis provided additional useful information. This is illustrated by Patient 1, who had equal interhemispheric tracer distribution despite the presence of a large malformation in one hemisphere. This suggested the coexistence of porencephaly, which was identified on subsequent CT scanning. Within the involved cerebral hemisphere of Patient 1, 64% of the tracer was located in the AVM. This was the highest value recorded for children in this series with

similarly located malformations (59%, 50%, 57%, and 51% for Patients 5, 6, 8, and 9, respectively). If flow was diminished on both sides, curve analysis using this method would only show any redistribution between the two hemispheres but not the overall reduction. Finally, curve analysis was a means of comparing successive examinations in the same patient. The child with the great cerebral vein of Galen malformation (Patient 4) had two examinations a year apart, with curve analysis showing the interhemispheric distribution virtually unchanged but indicating a slight increase in preferential arteriovenous shunting through the malformation.

Six of the AVMs were supratentorial (Patients 1, 4, 5, 6, 8, 9), whereas three were in the posterior fossa (Patients 2, 3, 7). Only three AVMs originated from the middle cerebral arterial system. In some instances it was possible to predict the main route of venous drainage by both curve analysis and visual inspection of the dynamic study. With the great cerebral vein of Galen malformation, prompt drainage occurred into the deep central venous system before the superior sagittal sinus could be seen (Fig. 4), whereas in other patients there was a more circuitous route eventually leading to the superior sagittal sinus (Fig. 2).

The cerebral aneurysm resulted in little if any shift in interhemispheric flow despite its size. On the basis of delayed retention of contrast during angiography (Fig. 5), one might speculate that its flow rate was lower than in most AVMs of comparable size.

Seven of nine AVMs were detected by CT scanning following contrast administration but in only one was a vascular mass suspected before iothalamate injection. False-negative CT scans in patients with AVMs have been reported by others, especially on precontrast studies (*22–25*). Consequently contrast enhancement is advocated for CT scanning in patients suspected of harboring an AVM (*22,26,27*). Our series does not confirm the suggestion that CT scanning following contrast injection will have as high a detection rate for AVMs as dynamic scintigraphy (*26,28*). Furthermore a patient with an external-carotid input to his AVM may have a false-negative CT scan even after contrast administration, while his dynamic scintigraphic studies will be abnormal (*28*). The detection rate of cerebral aneurysms by CT scanning appears to be less than that for AVMs. Scotti et al. (*29*) demonstrated only 11 out of 58 aneurysms by CT scanning, although the presence and location of subarachnoid hemorrhages allowed them to predict the presence and probable location of aneurysms. The detection rate for cerebral aneurysms is probably about the same for CT and radionuclide studies.

Dynamic scintigraphy is the most effective screening test to detect AVMs; our one cerebral aneurysm, albeit a giant variety, was detected by both scintigraphy and CT scanning. To favor optimal detection, the proper choice of anterior or posterior positioning for dynamic imaging is important. In most circumstances clinical features will direct this choice, although sometimes both studies will have to be performed (i.e., in ventricular hemorrhage). Delayed scintigraphy had three false-negative results while CT scanning had two (one patient falsely negative on both) which is interesting since both are static rather than dynamic examinations. Besides the advantage of accuracy, radionuclide studies were less expensive and did not require iodinated contrast agents. Furthermore, neither general anesthesia nor heavy sedation was needed. CT scanning, with its need for absolute patient immobility, may require such measures in children.

ACKNOWLEDGMENTS

The authors gratefully acknowledge the angiographic expertise of Philip Stanley, M.D. and John H. Miller, M.D. of Childrens Hospital of Los Angeles and Edward Helmer, M.D. of Kaiser Hospital of Los Angeles. The permission of Alfonso Carranza, M.D. of Childrens Hospital of Los Angeles to use the gross specimen in Fig. 5 is greatly appreciated.

FOOTNOTE

* From upswing to first peak, as before.

REFERENCES

1. OLDENDORF WH: Clinical applications of brain blood flow studies. *Semin Nucl Med* 1: 107–119, 1971

2. GATES GF: Computer assisted radionuclide evaluation of cerebral perfusion in children. Proceedings of the Sixth Annual Symposium on Sharing of Computer Programs and Technology in Nuclear Medicine, Howard BY, ed. New York, Society of Nuclear Medicine, 1976, pp 204–212

3. ROSENTHALL L: Intravenous and intracarotid radionuclide cerebral angiography. *Semin Nucl Med* 1: 70–84, 1971

4. BUDINGER TF, DELAND FH, DUGGAN HE, et al: Dynamic time-dependent analysis and static three-dimensional imaging procedures for computer-assisted CNS studies. In *Noninvasive Brain Imaging: Computed Tomography and Radionuclides*, DeBlanc HJ, Sorenson JA, eds. New York, Society of Nuclear Medicine, 1975, pp 45–66

5. SAPIRSTEIN LA: Measurement of the cephalic and cerebral blood flow fractions of the cardiac output in man. *J Clin Invest* 41: 1429–1435, 1962

6. MOSES DC, NATARAJAN TK, PREVIOSI TJ, et al: Quantitative cerebral circulation studies with sodium pertechnetate. *J Nucl Med* 14: 142–148, 1973

7. WAGNER HN: Cerebral circulation. *Nuclear Medicine*, Wagner HN, ed. New York, HP Publishings (adapted from *Hospital Practice*), 1975, 94–101

8. PENNING L, FRONT D: *Brain scintigraphy*. Amsterdam, Excerpta Medica-Amsterdam, 1975, pp 83–85

9. RAY BS: Cerebral arteriovenous aneurysms. *Surg Gynec Obstet* 73: 615–648, 1941

10. DeLand FH: *Cerebral Radionuclide Angiography*. Philadelphia, W B Saunders, 1976, pp 189–201

11. Young LW: Radiological case of the month: Vein of Galen malformation. *Am J Dis Child* 131: 581–582, 1977

12. Sostre S: Vein of Galen malformation. *Clin Nucl Med* 1: 211–212, 1976

13. Schurr PH, Wickbom I: Rapid serial angiography: Further experience. *J Neurol Neurosurg Psychiat* 15: 110–118, 1952

14. Tönnis W, Schieffer W, Walter W: Signs and symptoms of supratentorial arteriovenous aneurysms. *J Neurosurg* 15: 471–480, 1958

15. Häggendal E, Inguar DH, Lassen NA, et al: Pre- and postoperative measurements of regional cerebral blood flow in three cases of intracranial arteriovenous aneurysms. *J Neurosurg* 22: 1–6, 1965

16. Lassen NA, Høedt-Rasmussen K, Sørensen SC, et al: Regional cerebral blood flow in man determined by Krypton 85. *Neurology* 13: 719–727, 1963

17. Nylin G. Silfverskiöld BP, Löfstedt S, et al: Studies on cerebral blood flow in man, using radioactive-labelled erythrocytes. *Brain* 83: 293–336, 1960

18. Landman S, Ross P: Radionuclides in diagnosis of arteriovenous malformations of the brain. *Radiology* 108: 635–639, 1973

19. Waltimo O, Eistolia P, Vuolio M: Brain scanning in detection of intracranial arteriovenous malformations. *Acta Neurol Scand* 49: 434–442, 1973

20. Gates GF, Dore EK, Taplin GV: Interval brain scanning with sodium pertechnetate Tc-99m for tumor detectability. *JAMA* 215: 85–88, 1971

21. McDonald CA, Korb M: Intracranial aneurysms. *Arch Neurol Psychiat* 42: 298–328, 1939

22. Baker HL, Houser OW: Computed tomography in the diagnosis of posterior fossa lesions. *Radiol Clin No Amer* 14: 129–147, 1976

23. Fordham EW: The complementary role of computerized axial transmission tomography and radionuclide imaging of the brain. *Semin Nucl Med* 7: 137–159, 1977

24. Lukin RR, Chambers AA, Tomsick TA: Cerebral vascular lesions: infarction, hemorrhage, aneurysm, and arteriovenous malformation. *Semin Roentgenol* 12: 77–89, 1977

25. Terbrugge K, Scotti G, Ethier R, et al: Computed tomography in intracranial arteriovenous malformations. *Radiology* 122: 703–705, 1977

26. Alderson PO, Gado MH, Siegel BA: Computerized cranial tomography and radionuclide imaging in the detection of intracranial mass lesions. *Semin Nucl Med* 7: 161–173, 1977

27. Pinto RS, Becker MH: Computed tomography in pediatric diagnosis. *Am J Dis Child* 131: 583–592, 1977

28. Gado M, Coleman RE, Alderson PO: Clinical comparison of radionuclide brain imaging and computerized transmission tomography, I. *Noninvasive Brain Imaging: Computed Tomography and Radionuclides*, DeBlanc HJ, Sorenson JA, eds. New York, Society of Nuclear Medicine, 1975, pp 147–171

29. Scotti G, Ethier R, Melancon D, et al: Computed tomography in the evaluation of intracranial aneurysms and subarachnoid hemorrhage. *Radiology* 123: 85–90, 1977